INFLUENCE OF DESIGN PARAMETERS ON THE UNSTEADY FLOW IN A CENTRIFUGAL FAN

M. Younsi
Laboratoire d'Energétique et de Mécanique des Fluides Interne
mohand.younsi@paris.ensam.fr

F. Bakir
Laboratoire d'Energétique et de Mécanique des Fluides Interne
Farid.bakir@paris.ensam.fr

S. Kouidri
Laboratoire d'Energétique et de Mécanique des Fluides Interne
smaine.kouidri@paris.ensam.fr

R .Rey
Laboratoire d'Energétique et de Mécanique des Fluides Interne
robert.rey@paris.ensam.fr

ABSTRACT

The aim of this study is to evaluate the influence of design parameters on the unsteady flow in a forward-curved centrifugal fan and their impact on the aeroacoustic behavior. To do so, numerical and experimental study has been carried out on four centrifugal impellers designed with various geometrical parameters. The same volute casing has been used to study these fans. The effects on the unsteady flow behavior related to irregular blade spacing, blade number and radial distance between the impeller periphery and the volute tongue have been studied.

The numerical simulations of the unsteady flow have been carried out using Computational Fluid Dynamics tools (CFD) based on Unsteady Reynolds Averaged Navier Stokes approach (URANS). The sliding mesh technique has been applied at the interfaces between the rotating and stationary zones in order to model the blades' motion relative to the volute casing. The study is focused on the unsteadiness induced by the aerodynamic interaction between the volute and the rotating impeller blades. In order to predict the acoustic pressure at far field, the unsteady flow variables provided by the CFD calculations (pressure and velocity fluctuations acquired upon the surfaces of the rotating blades) have been used as inputs in the Ffowcs Williams-Hawkings equations (FW-H). Using this model, the acoustic pressure has been computed at the fan exit duct.

The experimental part of this work concerns measurement of aerodynamic performance of the fans using a test bench built according to ISO 5801 [1] standard. In addition to this, pressure microphones have been flush-mounted on the volute tongue surface in order to measure the wall pressure fluctuations. The sound pressure level (SPL) measurements have been carried out in an anechoic room in order to remove undesired noise reflections. Finally, the numerical results have been compared with the experimental measurements and a correlation between the wall pressure fluctuations and the far field noise signals has been found.

Keywords: Centrifugal Fan, CFD, Turbomachinery, Unsteady flow.

INTRODUCTION

Forward-curved centrifugal fans are widely used in industry for their large mass flow rate and their compactness compared to axial fans. Despite their low efficiency, they are employed as circulating fans in central heating and air-conditioning systems in buildings, as blowers in automotive heating-cooling units and in numerous other applications.

The recent development of CFD techniques for three dimensional viscous flow fields provides efficient tool for analysis and design. Thus, flow analysis techniques using URANS approach have made remarkable progress in turbomachinery applications.

Recently, more attention has been paid to the study of design parameters' effects on the performance and noise of centrifugal fans. Boltezar et al. [2] studied the influence of irregular blade spacing of car alternator radial fans on the total SPL and the noise spectrum. In their study, they computed the SPL and spectra theoretically and compared the values to measured results for several types of fans with different blade spacing. They found that alterations in blade spacing do not significantly alter the total SPL. However, significant dispersion of the sound power over several harmonics was found with irregular fan blade spacing, thus allowing for a reduction of the siren effect. They predicted this phenomenon theoretically and confirmed it experimentally. Jeon [3] used the discrete vortex method (DVM) to describe the flow field in a centrifugal fan. He employed the Lowson's [4] equation in order to obtain acoustic far field information from the unsteady force fluctuations on the blade. The purpose of his study is to investigate the effects of rotating velocity, flow rate, cut-off distance and number of blades on the noise of a centrifugal fan. Moon et al. [5] used the unsteady viscous flow fields of a cross-flow fan computed by solving the two dimensional (2D) incompressible Navier-stokes equations. They employed the FW-H equation in order to predict the acoustic pressures and to study the acoustic benefit of an impeller with uneven blade spacing. Tajadura et al. [6] performed a three-dimensional numerical simulation of the complete unsteady flow in the whole impeller-volute configuration of an industrial centrifugal fan. They obtained the pressure fluctuations in some locations over the volute wall and they found a good agreement between the numerical and the experimental results.

In this study, numerical and experimental approach is used to evaluate the influence of design parameters on the unsteady flow in a centrifugal fan and their impact on the aeroacoustic behavior.

NOMENCLATURE

a_0 Far field sound speed [m/s]

$f = 0$ Function that describes the source surface: impeller blades surfaces [-]

F Frequency [Hz]

G Green's function $= \tau - t + r/c$ [-]

$H(f)$ Heaviside function [-]

k Blades distribution coefficient [-]

M Local Mach number vector of source with respect to a frame fixed to the undisturbed medium, with components M_i [-]

N Rotational speed [rpm]

n Blades repetition number [-]

n_j Unit normal vector [-]

p' Acoustic pressure [Pa]

P_{ij} Compressive stress tensor [Pa]

p_{ref} Reference pressure [Pa]

r Distance between observer and source [m]

R_2 Impeller outlet radius [m]

t Observer time [s]

T_{ij} Lightill stress tensor [Pa]

u_i Fluid velocity in the x_i direction [m/s]

u_n Fluid velocity in the normal direction [m/s]

v_i Surface velocity in the x_i direction [m/s]

v_n Surface velocity in the normal direction [m/s]

x Observer position vector [m]

z Blades number

$\delta(f)$ Dirac delta function [-]

ΔP_s Static pressure generated by the fan [Pa]

ΔS Cell grid size at the impeller periphery [mm]

Δt Time step [s]

$\Delta \theta_b$ Blade pitch angle [degree]

ρ Density [kg/m^3]

τ Source time [s]

η Efficiency [%]

Subscripts

b Blade number

L   Loading noise component

T   Thickness noise component

0 Denotes fluid variable in quiescent medium

FANS PRESENTATION

In this study, four impellers (VA160, VA160D, VA150, VA160E), designed with various geometrical parameters have been investigated in the same volute casing. The VA160 impeller is considered as the reference. Compared to the VA160, the VA160D presents irregular blade spacing, the VA150 has different impeller outlet diameter (150 mm) and the VA160E gives smaller number of blades (19 blades). The main geometrical characteristics of the reference impeller and the volute casing are presented in Table 1.

Reference impeller VA160	
Description	*Value*
Blade number	39
Impeller width	70 mm
Blade chord length	26.2 mm
Blade thickness	1 mm
Inlet blade angle	5°
Outlet blade angle	70°
Shape blade	circular arc
Impeller inlet diameter	120 mm
Impeller outlet diameter	160 mm
Rotational speed	3000 rpm.
Volute casing	
Inlet diameter	120 mm
Outlet size	100 x 76 mm
Volute tongue radius	5 mm
Volute tongue position	Radius 90 mm
Volute shape	Logarithmic law

Table1. Geometrical characteristics of the reference fan.

Concerning the VA160D impeller, the blades pitch distribution has been obtained using the following equation proposed by the present paper authors:

$$\Delta\theta_b = \frac{360}{z} + k\left[\left(\frac{z}{2\pi.n}\right)\left\{\cos\left[\left(\frac{n\times 2\pi}{z}\right)\left(b-\frac{1}{2}\right)\right]\left(\frac{\pi}{180}\right)\right\}\right] \quad (1)$$

Where: $k = 50$; $z = 39$; $n = 3$.
This equation gives the blade's pitch angle as a sinusoidal function of the blade number (b) (see Figure 2). The VA160 fan has a constant blade pitch angle of 9.23 deg.
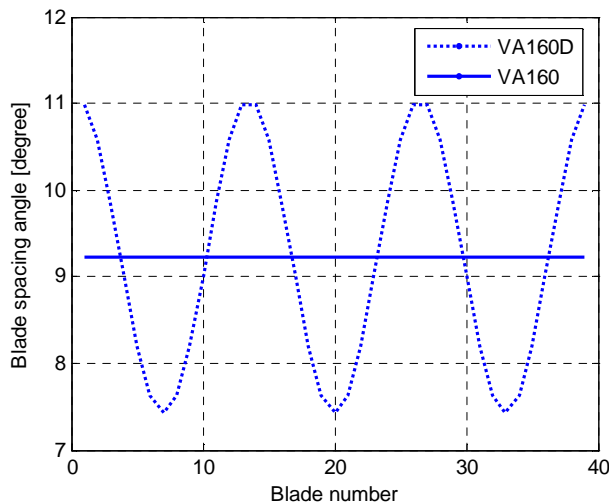
Figure 2. Blade pitch angle distributions
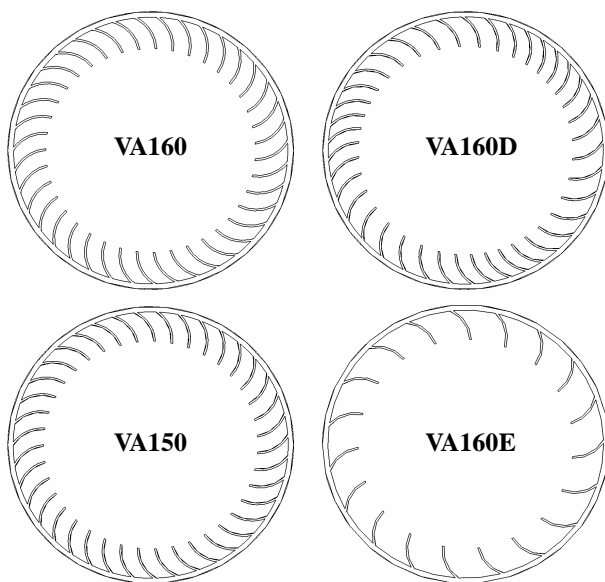
Figure 3. Geometry of the investigated fans

Figure 3 shows the geometry for the four impellers under consideration. These parameters have been transformed into complete 3D Computer Aided Design model (CAD) in order to build prototype for the experimental investigations.

EXPERIMENTAL WORK

Overall measurements have been carried out on the test bench shown in Figure 4, designed and built at LEMFI-ENSAM according to the ISO 5801 standard. It is composed of an airtight box (1.3 x 1.3 x 1.8 m), which is placed upstream the centrifugal fan, making possible to vary the flow rate by changing the diameter of an orifice plate (diaphragm). The rotational speed is set by a frequency converter and measured using an optical tachometer of 0.1% accuracy. For each diaphragm of given diameter, the static pressure provided by the centrifugal fan is measured using a micro manometer (precision 1%). The experimental work also consists of the measurements of wall pressure fluctuations in the volute casing. Thus, one *AREVA 01dB-Metravib 40BH ¼ in.* pressure microphone which presents +/- 0.2dB uncertainty has been flush-mounted on the volute tongue surface. Additionally, *one AREVA 01dB-Metravib 40AE ½ in.* free field microphone with +/- 0.2dB uncertainty, protected with a nose cone, has been used in order to measure the acoustic pressures. These acoustic measurements have been performed in anechoic room (5.9 x 4.4 x 4.25 m). Background sound pressure level is 18 dB and cut-off frequency is 75 Hz. In order to make possible these measurements, the fan has been adapted on a small airtight box (0.6m x 0.6m x 0.6m) and the conformity to the ISO 5801 standard has been checked. One free field microphone has been positioned one meter away from the fan rotational axis, in the same direction of the exit duct (see Figure 5). After the calibration operations, the signals from the microphones have been introduced into a personal computer using an analog-to-digital board, and post-processed using narrow band width analysis.

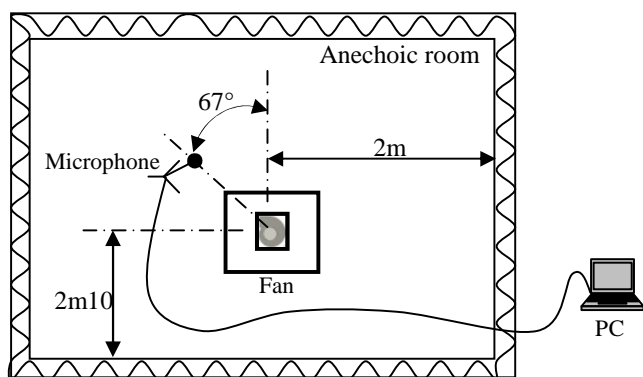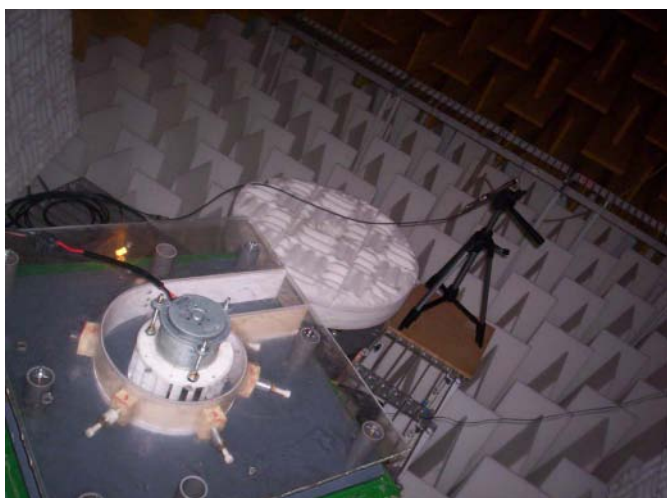**Figure 4. Test bench and pressure fluctuations measurements**

3

Figure 5. Acoustic measurements

Figure 6. Geometry modeling of the flow domains

In order to compare the unsteady flow behavior of the investigated fans at the same design point (500 m^3/h, 680 Pa), the fans rotational speed have been determined experimentally. Thus, the rotational speed of the VA160, VA160D, VA150 and VA160E are set to 3000 rpm, 3000 rpm, 3200 rpm and 2900 rpm respectively.

NUMERICAL MODELING

To consider the unsteady interactions between the rotating impeller blades and the stationary fan casing and to understand the internal flow, a numerical simulation based on the finite volume numerical method using *FLUENT 6.2* code has been carried out. The geometrical parameters given in Table1 have been used in order to generate the computational domain which has been divided into two zones, a rotational zone including the impeller and stationary zone elsewhere. This configuration takes into account the clearance between the impeller and the volute. The inlet and the outlet surfaces of the fan have been extended in order to ensure numerical stability and to minimize boundary conditions effects. The obtained computational domains are shown in Figure 6.
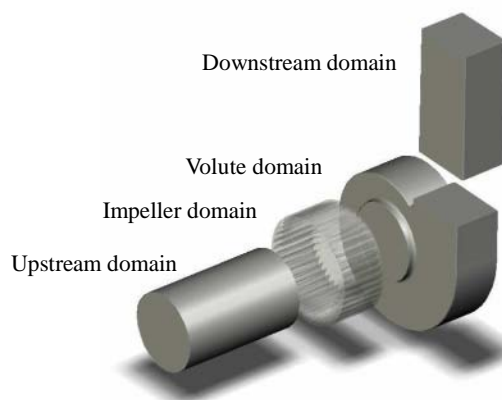
The resulting geometry has been used to build a hybrid mesh. The grid refinement has been studied and adapted to the flow morphology, minimizing element distortion and to achieve required resolution in high gradient regions. The details of this study are reported in previous papers by Younsi et al. [7, 8]. An example of the retained grid mesh is shown in Figure 7. The meshes generated for all the four fans contain approximately 2 million elements.
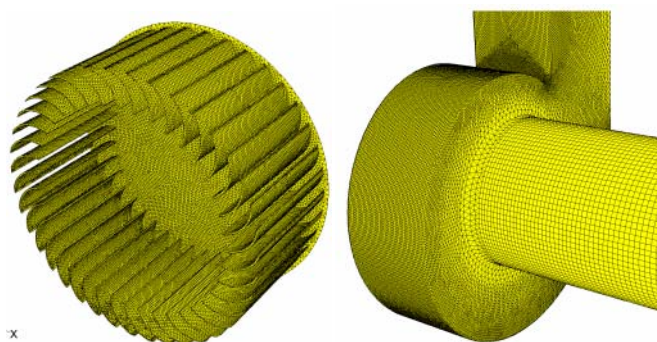

Figure 7. Retained grid mesh for the VA160 fan

Concerning the numerical simulation parameters, Velocity Inlet and Pressure Outlet boundary conditions have been applied at the inlet and the outlet respectively. Majidi [9] suggested that the assumption of a fixed mass flow rate at the inlet of the computational domain is physically unsuitable for unsteady calculations and in particular for considering the rotor/stator interaction. The sliding mesh technique has been applied to the interfaces in order to allow the unsteady interactions between the impeller and the volute casing. Turbulence has been modeled with the k-ω-SST model [10].

The SST model performance has been studied and validated in a large number of cases [11]. It has been shown to perform very well for adverse pressure gradient aerodynamic flows. The maximum residue is lower or equal to 10^{-4}. The governing equations have been solved using the segregated solver and a centred SIMPLE algorithm has been used for the pressure velocity coupling. The time-dependent term scheme is second order. A gauge pressure of 101325 Pascal has been applied at the outlet and a suitable value has been determined for the inlet. The CFD simulation process began with a steady flow calculation using the Frozen-Rotor approach. In this case, the relative position of the impeller and casing does not change during the calculations. For unsteady calculations, the grids change their relative position during the calculations according to the angular velocity of the impeller. The time step of the unsteady calculations has been set to 5.10^{-5} seconds. The chosen time step is related to the rotational speed of the impeller and it is small enough to get the necessary time resolution and to capture the phenomena due to the blades passage and their interactions with the volute casing wall. It corresponds to 1/400 of blade passing period. This time step has been approached by the following formulation:

$$\Delta t \cong \frac{30 \cdot \Delta S}{\pi \cdot N R_2} \qquad (2)$$

Where ΔS is set to 2 mm.

The unsteady calculations are carried out for seven impeller revolutions and the obtained temporal data have been saved for each time step. After windowing the temporal signals using Hamming's window function, each recorded sample has been Fast Fourier Transform (FFT) processed ($P_{ref} = 2\times10^{-5}$ Pa), and then the aerodynamic pressure spectra have been finally obtained.

AEROACOUSTIC CALCULATIONS

The (FW-H) equation [12, 13] is essentially an inhomogeneous wave equation that can be derived manipulating the continuity equation and the Navier-Stokes equations. The FW-H equation can be written as:

$$\frac{1}{a_0^2}\frac{\partial^2 p'}{\partial t^2} - \nabla^2 p' = \frac{\partial [[\rho_0 v_n + \rho(u_n - v_n)]\delta(f)]}{\partial t}$$
$$- \frac{\partial [[P_{ij}n_j + \rho u_i(u_n - v_n)]\delta(f)]}{\partial x_i} + \frac{\partial^2}{\partial x_i \partial x_j}[T_{ij}H(f)] \qquad (3)$$

Where :
$$T_{ij} = \rho u_i u_j + P_{ij} - a_0^2(\rho - \rho_0)\delta_{ij} \qquad (4)$$

$$P_{ij} = p\delta_{ij} - \mu\left[\frac{\partial u_i}{\partial x_j} + \frac{\partial u_j}{\partial x_i} + \frac{2\partial u_k}{3\partial x_k}\delta_{ij}\right] \qquad (5)$$

The first two source terms in equation (3) are monopole (thickness) and dipole (loading) sources, respectively, based on their mathematical structure. The monopole source term models the noise generated by the displacement of fluid as the body passes. The dipole or loading source term models the noise that results from the unsteady motion of the force distribution on the body surface. Both of these sources are surface sources: i.e., they act only on the surface $f=0$ as indicated by the Dirac delta function $\delta(f)$. The third source term is a quadripole source term that acts throughout the volume that is exterior to the data surface as indicated by the Heaviside $H(f)$.

Using the free-space Green's function, $(\delta(G)/4\pi$; with $G=\tau-t+r/a_o)$ the solution to equation (3) is obtained. Thus the complete solution consists of surface integrals and volume integrals. The surface integrals represent the contribution from monopole and dipole acoustic sources and partially from quadrupole sources if the integration surface is impermeable. The contribution of the volume integrals which represent quadrupole (volume) sources in the region outside the source surface becomes small when flow is subsonic. Thus the volume integrals are neglected.

Finally:

$$p'(\vec{x},t) = p'_T(\vec{x},t) + p'_L(\vec{x},t) \qquad (6)$$

The two terms on the right in equation (6), $p'_T(\vec{x},t)$ and $p'_L(\vec{x},t)$, thickness and loading terms respectively are given by:

$$4\pi p'_T(\vec{x},t) = \int_{f=0}\left[\frac{\rho_0(\dot{U}_n + U_{\dot{n}})}{r(1-M_r)^2}\right]dS$$
$$+ \int_{f=0}\left[\frac{\rho_0 U_n\{r\dot{M}_r + a_0(M_r - M^2)\}}{r^2(1-M_r)^3}\right]dS \qquad (7)$$

$$4\pi p'_L(\vec{x},t) = \frac{1}{a_0}\int_{f=0}\left[\frac{\dot{L}_r}{r(1-M_r)^2}\right]dS$$
$$+ \int_{f=0}\left[\frac{L_r - L_M}{r^2(1-M_r)^2}\right]dS \qquad (8)$$
$$+ \frac{1}{a_0}\int_{f=0}\left[\frac{L_r\{r\dot{M}_r + a_0(M_r - M^2)\}}{r^2(1-M_r)^3}\right]dS$$

Where:

$$U_i = v_i + \frac{\rho}{\rho_0}(u_i - v_i)$$

$$L_i = P_{ij}\hat{n}_j + \rho u_i(u_n - v_n)$$ (9)

The square brackets in Equations (7) and (8) denote that the kernels of integrals are computed at the corresponding retarded times, it is defined as follows:

$$\tau = t - \frac{r}{a_0}$$ (10)

The various subscripted quantities appearing in Equations (7) and (8) are the inner products of a vector and a unit vector implied by the subscript. For example:

$$L_r = \vec{L}.\vec{r} = L_i r_i \quad \text{and} \quad U_n = \vec{U}.\vec{n} = U_i n_i$$

Where $\vec{r}$ and $\vec{n}$ denote the unit vectors in the radiation and wall normal directions respectively. The dot over a variable denotes source-time differentiation of that variable.

Using the URANS calculations after the statistical variables stability, the fluctuating variables, (pressure and velocity) upon the impeller surfaces, have been extracted for 2000 time steps. Then, sound pressure signals are computed at the receiver location using the source data collected during the aerodynamic calculations. It is important to state that the presence of the volute casing is neglected in this approach (free field radiation). For this reason, the acoustic pressure calculations have been carried out at the position shown in Figure 8.
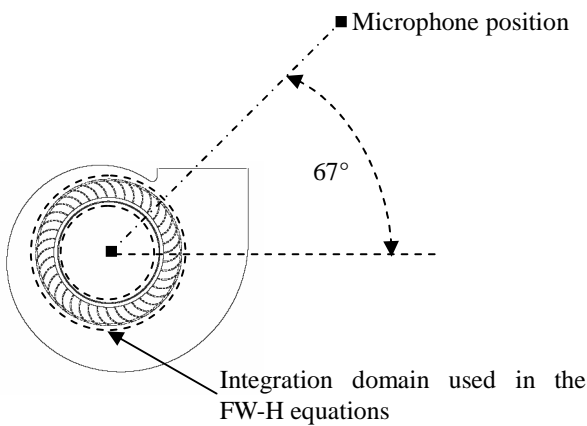

Figure 8. Position of the acoustic pressure calculations and integration domain

AERODYNAMIC RESULTS AND DISCUSSION

The aerodynamic characteristics of the studied fans are given in Table 2. It can be seen that the VA160D fan (with irregular blades spacing) has the same characteristics as the reference fan (VA160). This result indicates that alterations in blades spacing do not significantly alter the aerodynamic characteristics of the fan.

Compared to the other fans, the VA150 presents a better efficiency because of its smaller outlet radius which contributes to minimize the total moment applied on the rotating blades. However, the pressure decrease is compensated by increasing the rotational speed until 3200 rpm. In addition to this, the VA160E fan presents a better efficiency compared to the VA160 and VA160D fans. Indeed, reducing the number of blades contributes to minimize aerodynamic losses through the impeller blades grid. Then, to generate the requested fan characteristic (680Pa), the impeller rotational speed is decreased to 2900 rpm.
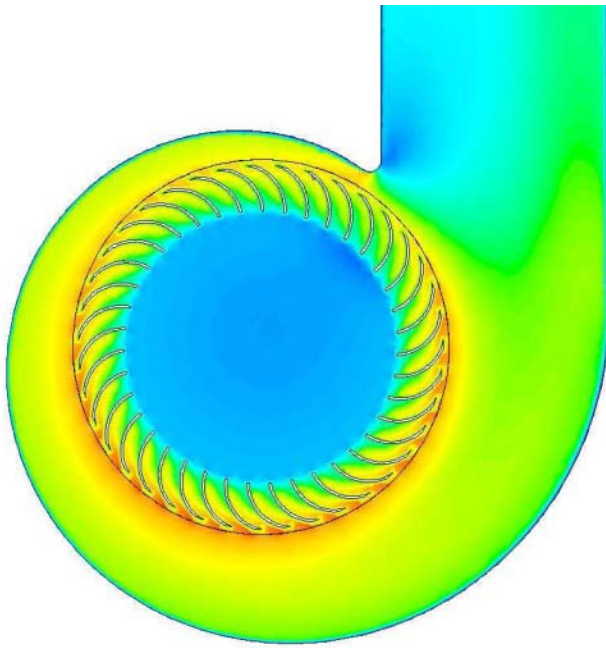
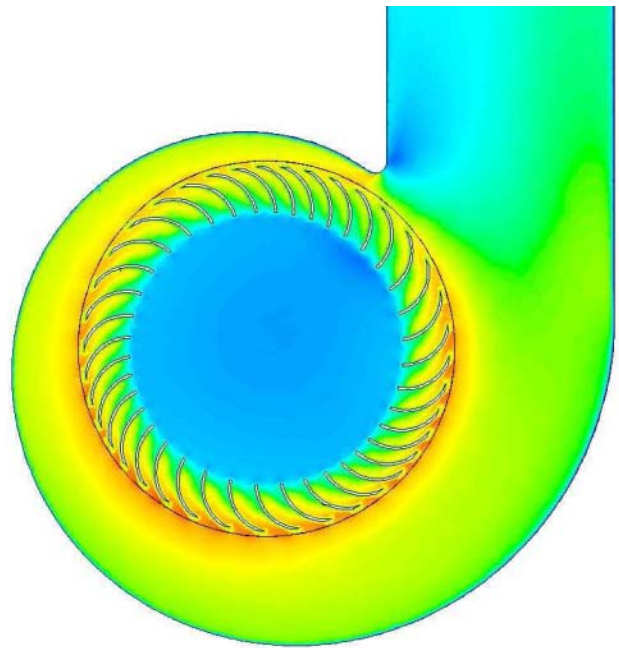| Fan	N (rpm)	ΔP_s (num.)	ΔP_s (exp.)	η (%)
VA160	3000	682	681	51
VA160D	3000	679	680	51
VA150	3200	700	684	54
VA160E	2900	640	678	52

Table 2. Aerodynamic characteristics

Figures 9 shows the instantaneous velocity field at the median surfaces of the VA160, VA160D, VA150 and VA160E fans respectively. According to these figures, the conversion of dynamic pressure produced by the impeller rotation into static pressure by the volute casing can be seen. A non homogenous velocity distribution is observed at the zone around the gap between volute tongue and impeller periphery, characterized by a high gradient of velocity. The volute tongue whose role is to drive the flow towards the fan outlet also presents a singularity for the flow. The shape of the volute casing creates a geometrical asymmetry which influences the velocity and pressure distribution.

The comparison between the VA160 and VA160D fans shows that alterations in blades spacing do not significantly alter the overall flow field of the fan. On the other hand, the VA150 fan presents more homogenous flow field around the impeller periphery and particularly at the volute tongue zone. In this configuration, the interactions between the volute tongue and the rotating blades are minimized by reducing the radial distance between the volute tongue and the impeller periphery.
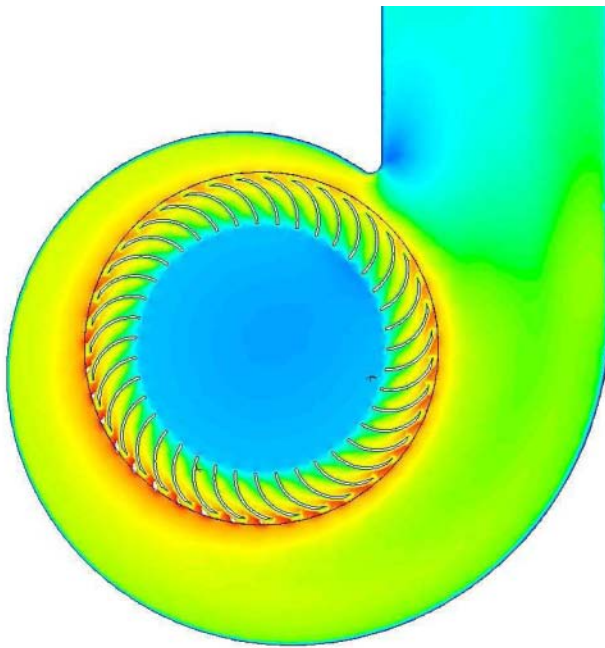
According to the figure 9, the VA160E with smaller number of blades, generates a non homogenous flow field particularly at the impeller periphery. A similar result has been shown in [14] concerning the influence of the blades number on the flow field of a centrifugal pump.
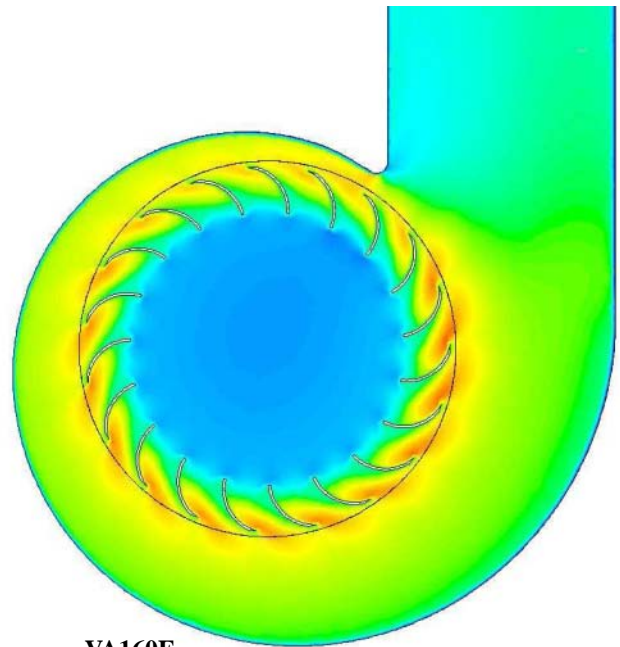
6 Copyright © 2007 by ASME

VA160

VA160D

VA150

VA160E

48.0 46.1 44.6 43.2 41.7 40.3 38.9 37.4 36.0 34.6 33.1 31.7 30.2 28.8 27.4 25.9 24.5 23.0 21.6 20.2 18.7 17.3 15.8 14.4 13.0 11.5 10.1 8.6 7.2 5.8 4.3 2.9 1.4 0.0

Figure9. Instantaneous velocity field at the meridian surface (0.14 s)

7   Copyright © 2007 by ASME

WALL PRESSURE FLUCTUATIONS AND SPECTRAL ANALYSIS

The time histories of the pressure fluctuation at the investigated nodal points on the volute tongue are shown in Figure 10 with their corresponding spectral analysis. The numerical results are compared to the experimental data. Concerning the VA160 and VA150 fans, a good agreement has been found between the measured data and the numerical calculations particularly at the blade passing frequency (BPF) and at lower frequencies. The spectra of the pressure fluctuation level computed and measured on these fans suggest that the dominant mode occurs at 1950 Hz and 2080 Hz respectively. These frequencies correspond to the BPF point. Absence of other dominant peaks in the spectra at the harmonic frequencies is observed. This is due to the nature of the interaction between the impeller and the volute tongue which generates small interferences. Thus, the corresponding harmonics are hidden by the broad band signal components. The main interactions which could produce tonal component in the signal are due to the presence of the volute tongue near the impeller periphery. The pressure fluctuation level at the BPF spectrum is higher for VA160 than VA150. The VA150 presents smaller radial distance between the impeller and the volute tongue and the aerodynamic interactions between the rotating and stationary zones are less important.

Concerning the VA160D fan behavior, the wall pressure fluctuations are underestimated by the measurements. For these high pressure fluctuations the pressure microphone is saturated and the real signal is not read adequately. However, the overall form of the experimental signal is in good agreement with the CFD predictions. Both these signals clearly show passage of all the three blade blocs per revolution which correspond to the three cycle pitch variation at 150 Hz. On the other hand, the split discrete frequencies are separated by multiples of 150Hz from the BPF.

Concerning the unsteady pressure generated by the VA160E fan, the phenomenon due to the microphone saturation is observed. Two high dominant peaks are observed at the BPF (950 Hz) and at the second harmonic frequency (1900 Hz). It can be seen that the pressure fluctuation level at these frequencies is higher for VA160E than VA150.

Finally, the analysis of the four spectra shows that the numerical and experimental data don't match beyond a certain frequency (around 4000 Hz). This cut-off frequency is related to the mesh resolution and it represents the upper limit of frequency resolvable by the used numerical modeling. Finer mesh grid coupled with Large Eddy Simulation (LES) calculations could improve the matching between these results.
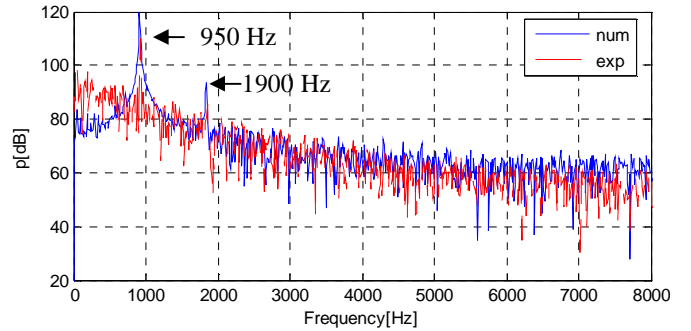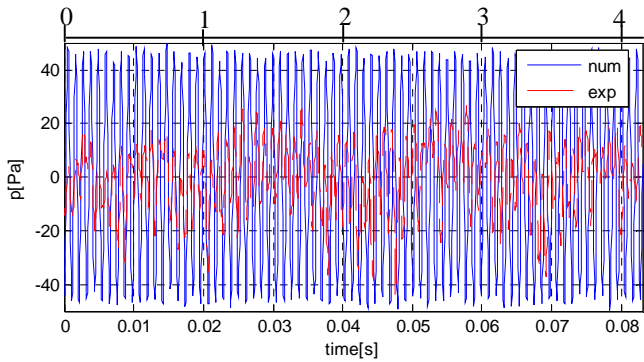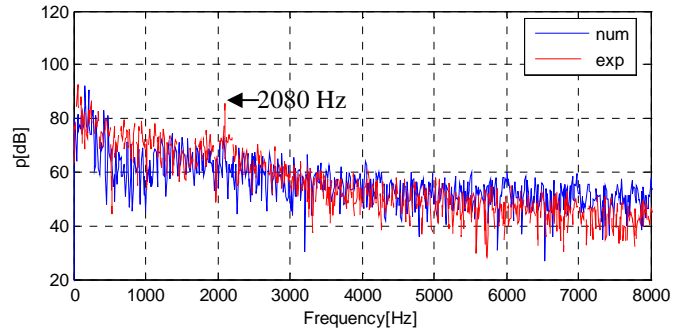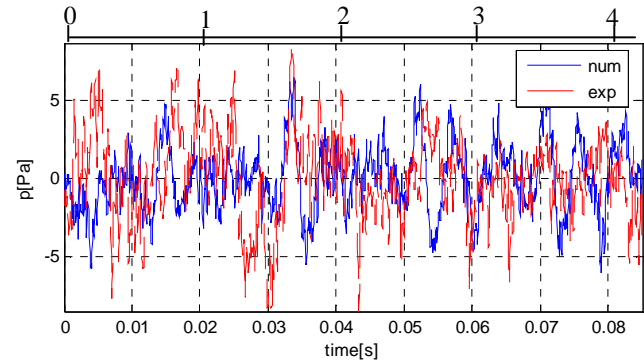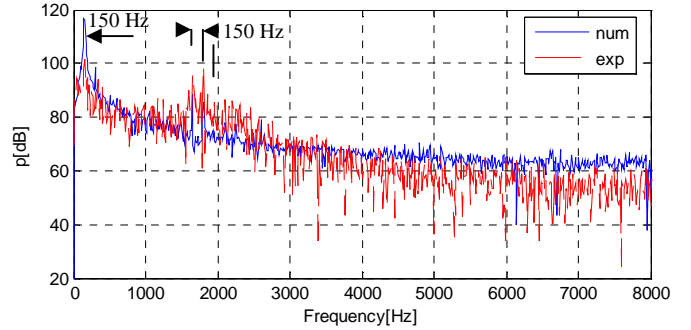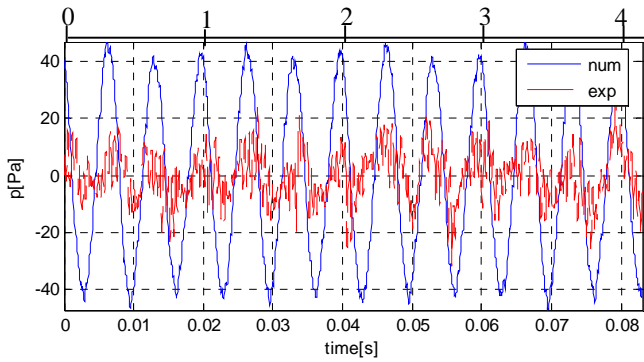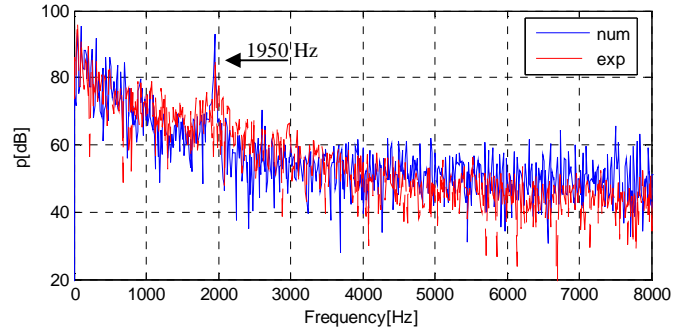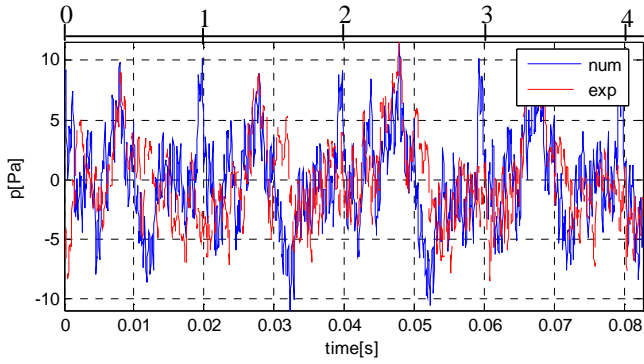
Figure 10. Wall pressure fluctuations with corresponding spectral analysis (VA160, VA160D, VA150 and VA160E)

ACOUSTIC RESULTS AND DISCUSSION

The acoustic signals generated by the four investigated fans are shown in figures 11-1, 11-2, 11-3 and 11-4 respectively. The experimental data are compared to the URANS/FW-H calculations. The analysis of these signals obtained at far field shows a correlation between the unsteady pressures acquired at near field and at the far field. Thus, the remarks cited in the wall pressure fluctuation level section are valid also in the present section. The four signals show two peaks at 300 Hz and 600 Hz respectively related to the fan motor signature which do not depend on the rotational speed.

Tables 3, 4, 5 and 6 show the comparison between the numerical and experimental results at the remarkable frequencies (BPF and their harmonics) of the investigated fans. It can be seen that the SPL values given by the numerical calculations are lower than the measured data (~ 5 to 8 dB). These differences partially represent the reflections and reverberations of the experimental facility which are not taken into account in the FW-H equation (free field radiation). On the other hand, the numerical modeling has not been used in order to predict the broadband noise. According to [13], URANS calculations cannot adequately provide the surface pressure fluctuations needed for broadband noise prediction. This remark explains the differences on the broad band signals components found between the numerical and the experimental results. Thus, the significant part of the predicted acoustic signals consists of the tonal noise generated by the flow unsteadiness and interactions between rotating blades and volute casing.

According to Table 4, the VA150 fan generates lower SPL than VA160 fan showing that reduction of the distance between the blade periphery and the volute tongue allows to minimize the generated tonal noise (~ 4 dB at the BPF).

Concerning the VA160E fan, it gives the highest SPL compared to the other fans. This result shows that the reduction of number of blades generates strong aerodynamic interactions (between volute tongue and rotating blades) which contribute to accentuate the tonal noise at the BPF.

VA150	Frequencies	SPL (dB)	
		EXP.	URANS/FW-H
	2080 Hz	53	45

Table 5. Numerical and experimental SPL value (VA150)

VA160E	Frequencies	SPL (dB)	
		EXP.	URANS/FW-H
	950 Hz	78	64
	1900 Hz	55	50

Table 6. Numerical and experimental SPL value (VA160E)

VA160	Frequencies	SPL (dB)	
		EXP.	URANS/FW-H
	1950 Hz	57	51

Table 3. Numerical and experimental SPL value (VA160)

VA160D	Frequencies	SPL (dB)	
		EXP.	URANS/FW-H
	1500 Hz	51	44
	1650 Hz	55	52
	1800 Hz	57	47

Table 4. Numerical and experimental SPL value (VA160D)
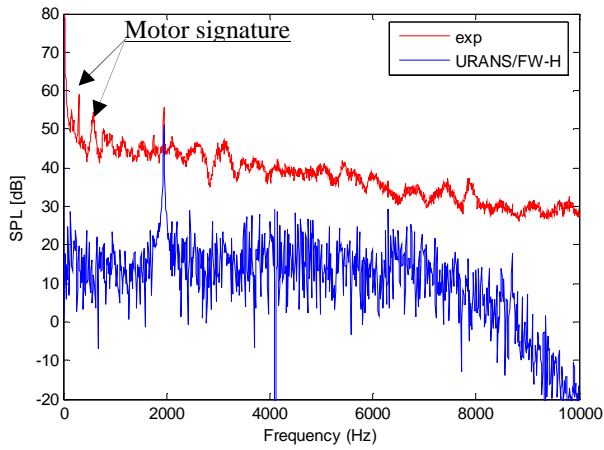
Figure 11-1. VA160 acoustic pressure (3000 rpm)
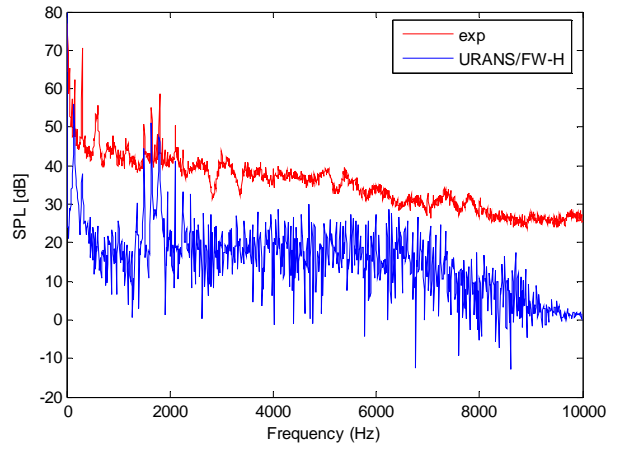

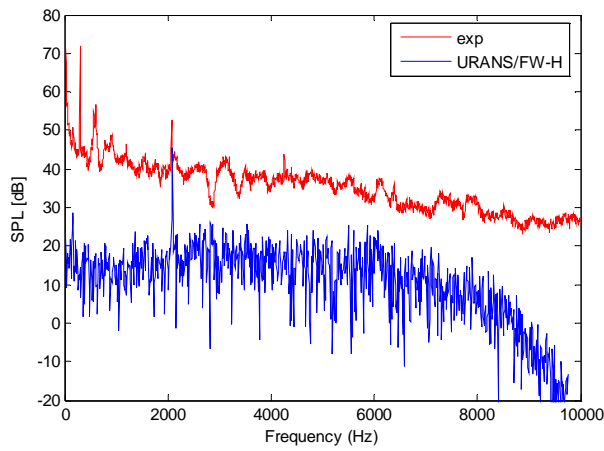**Figure 11-2. VA160D acoustic pressure (3000 rpm)**

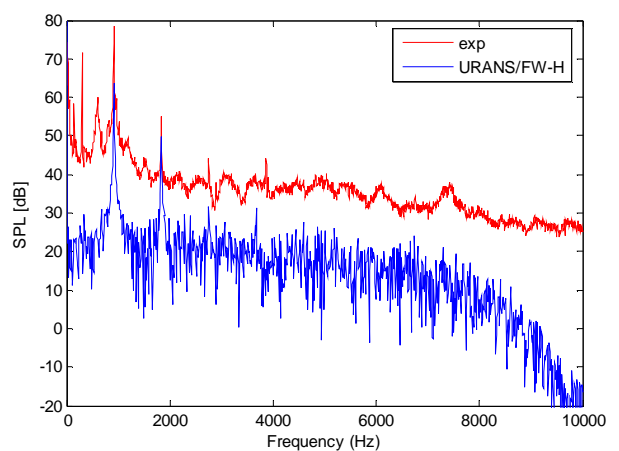**Figure 11-3. VA150 acoustic pressure (3200 rpm)**

Figure 11-4. VA160E acoustic pressure (2900 rpm)

CONCLUSION

Influence of design parameters on the unsteady flow in a centrifugal fan has been studied in this paper, using numerical and experimental investigations. The study showed the effects related to irregular blade spacing, blades number and radial distance between the impeller periphery and the volute tongue. A correlation between the wall pressure fluctuations and the far field noise signals has been found.

It should be interesting to extend this work by:

- Using Large Eddy Simulation (LES) approach to feed acoustic models.
- Using Laser Doppler velocimetry (LDV) and particle image velocimetry (PIV) technique in order to investigate the unsteady velocity field.

ACKNOWLEDGMENTS

REFERENCES

[1] ISO 5801, 1997, "Industrial fans - Performance testing using standardized airways".

[2] Boltezar M., Mesaric M., Kuhelj A., 1998, "The Influence of Uneven Blade Spacing on the SPL and Noise Spectra Radiated from Radial Fans", *Journal of Sound and Vibration*, 216(4), pp. 697-711.

[3] Jeon Wan-Ho, 2003, "A Numerical Study on the Effects of Design Parameters on the Performance and noise of a Centrifugal Fan", *Journal of Sound and Vibration*, 265, pp. 221-230

[4] Lowson M. V., 1965, "The Sound Field for Singularities in Motion", *Proceedings of the Royal Society in London*, Series A286, pp. 559-572.

[5] Cho Y., Moon Y-J, 2003, "Discrete Noise Prediction of Variable Pitch Cross-Flow Fans by Unsteady Navier Stokes Computations", *ASME Journal of Fluids Engineering*, Vol.125, pp.543-550.

[6] Tajadura R.-B., Suarez V.-S., Cruz J.-P.-H., and Morros C.-S, "Numerical calculation of pressure fluctuations in the volute of a centrifugal fan", *Journal of Fluids and Engineering*, 128, 2006, 359-369

[7] Younsi M., Bakir F., Kouidri S., Rey R., 2006, "2D and 3D Unsteady Flow in Squirrel-Cage Centrifugal Fan and Aeroacoustic Behavior", *Proceedings of FEDSM2006 ASME Joint U.S. - European Fluids Engineering Summer Meeting*, July 2006, Miami, FL USA

[8] Younsi M., Bakir F., Kouidri S., Rey R., 2007,"Numerical and Experimental Study of Unsteady Flow in Centrifugal Fan", 7th Europeen Turbomachinery Conference, Athens, Greece

[9] Majidi K., 2005,"Numerical Study of Unsteady Flow in a Centrifugal Pump", *Journal of Turbomachinery*, Vol. 127, pp 363-371

[10] Menter, F. R., 1993, "Zonal Two Equations k-ω Turbulence Models for Aerodynamic Flows", *AIAA paper*. 93-2906

[11] Bardina, J.E., Huang, T. J., and Coakley, 1997,"Turbulence Modeling, Validation, testing and development", *NASA Technical Memorandum* 110446

[12] Ffowcs Williams, J.E., Hawkings, D.L., 1969, "Sound Generation by Turbulence and Surfaces in Arbitrary Motion", *Phi. Trans. Roy. Soc.*, A264

[13] Brentner, K.S., Farassat, F., 1998, "An analytical Comparison of the Acoustic Analogy and Kirchhoff Formulation for Moving Surfaces", *AIAA Journal, 36(8)*.

[14] Kergourlay G., Younsi M., Bakir F., and Rey R., 2007 *"Influence of Splitter Blades on the Flow Field of a Centrifugal Pump: Test-Analysis Comparison,"* International Journal of Rotating Machinery, vol. 2007, Article ID 85024, 13 pages, doi:10.1155/2007/85024